DEGREE PROJECT

Harmonic Filters For Electronic Drive Systems Targeting Aircraft Applications

Emelie Berglund

Engineering Physics and Electrical Engineering, master's level
2023

Luleå University of Technology
Department of Computer Science, Electrical and Space Engineering

LULEÅ UNIVERSITY OF TECHNOLOGY

[This page intentionally left blank]

Abstract

Climate change pressures fossil-driven vehicles into electrification to sustain a healthy planet and environment for its inhabitants. Air traffic contributes to the ongoing climate crisis, and electric aircraft is taking its toll on the avionics market. The electrification of aircraft is complex and requires specialists and researchers to engage in the subject to haste the process of electric aircraft becoming commercial.

The electrification of aircraft comes with challenges in electromagnetic compatibility (EMC). Part of the aim of this study was to get a broad view of what EMC problems electric aircraft are facing. The leading purpose was to understand electric drive with brushless DC (BLDC) motors and to design and construct an active cancellation filter (ACF) for reducing harmonic noise in electric propulsion systems.

A literature study including recent research on EMC issues onboard, outside of, and within the system of electric aircraft deepened the view of the specifications and limits in the electronic design of the airplane. The literature study also covered electric propulsion using BLDC motors and ACF topologies for suppressing harmonics originating from the power inverter in the electric propulsion system.

Measurements on a Cypress motor kit with a BLDC motor showed ringings on the motor phase voltages. The parasitic drain-source capacitances in the MOSFETs of the motor inverter caused the ringings, and damping resistors managed to overcome the ringings in simulations and when measured. However, adding damping resistors line-to-line on the motor phase was determined to be ineffective, but the knowledge of the ringings and how to manage them will become relevant for future work.

This study proposed an ACF and a hybrid filter for attenuating harmonics caused by a square wave. The proposed hybrid filter was the ACF filter with an LC filter added to it. Simulations showed that the ACF suppresses harmonics up to 2 MHz, and the hybrid filter had no impact. The measured results showed that the ACF and hybrid filter suppress harmonics up to 10 MHz, and beyond 10 MHz, the filters stop the attenuation of harmonics. The purpose of the hybrid filter was to eliminate harmonics in the higher frequency band, where the performance of the ACF started to lack. However, the hybrid filter showed no influence on the ACF performance, which might have been due to software issues with the Fourier transform.

Although the filters did attenuate harmonics from the voltage pulse source, it could not be stated whether the ACF and hybrid filter topology will perform the same when applied to the drive system of an electric aircraft. Future work will determine how the filters perform on the Cypress motor kit, and eventually, with electric aircraft.

Contents

1 Introduction

Climate change has been a hot topic over decades, and modern technology has come to strive for zero emissions. Thus, fossil-driven vehicles are starting to be outnumbered by electric ones. The electrification of vehicles also concerns aircraft, though electric aircraft have not come as far as electric cars. The European Commission states that of the total CO2 emissions of 2017, 3.8 % were due to air traffic. CO2 emissions are not only a concern since aviation also emits nitrogen oxides, water vapor, and sulfate and soot particles, which affect the climate negatively [1]. According to the European Commission's avionics milestones, commercial aviation (with less than 70 seats) should be fully electrified by 2055. Larger aviation (more than 70 seats) should have at least 30 % hybridization for power and at least 10 % hybridization for stored energy. Personal aircraft and drones expect to be fully electrified by 2035 [2].

Electric aircraft face power supply and weight issues, which limit travel distance and prevent electric aircraft from being flown commercially [3]. On the other hand, the Swedish industrial enterprise Heart Aerospace is developing the ES-30, a 30-passenger airplane with an expected pure electric travel distance of 300 km by the late 2030s [4].

1.1 Problem Statement

Electric aircraft is a fundamental building block in our way toward making a massive positive environmental impact. However, common-mode (CM) electromagnetic noise and harmonics may inhibit the reliability and safety of electric air transportation. The purpose of this thesis is to investigate the EMC issues in electric aircraft, which further narrows down to electric propulsion systems and their CM voltage characteristics and active cancellation filter (ACF) design.

The workflow needs to be dissolved into parts to achieve results, starting with the basics in order to enable advancement toward practical implementations. Initially, a brief literature review covering noise related to electric avionics internally and externally will broaden the insight into electromagnetic and harmonic interference in electric air transportation.

The CM voltage of the inverter is a part of the inverter's nature of noise, and how to define and measure it for a brushless DC (BLDC) motor system will be investigated.

Driving BLDC motors and knowing the origin of harmonic noise are the key parts to understanding the necessity of an ACF. A three-phase BLDC enclosed with a motor inverter is the system that is tackled in this study. However, because of its complexity, a three-phase ACF design and implementation on the three-phase motor system is out of the scope of this study. Therefore, the work of this thesis only proposes and tests a single-phase ACF configuration.

2 Theory

This section is a literature review that will introduce background on electromagnetic compatibility (EMC) challenges internally, externally, and onboard in regular and electrified aircraft. Recent research regularly discusses internal issues such as electromagnetic interference (EMI) and wiring in electric aircraft, which is increasing due to electrification. Inverter topologies and their advantages for reducing weight and harmonics and increasing efficiency are central to the recent research regarding internal electronic systems in electrified aircraft.

Regular aircraft research has covered external occurrences, like lightning and on-ground communication facilities, and onboard electronic devices brought by passengers in commercial aircraft. However, the advancement in electronics due to electrification makes researchers reconsider the already debated topics in conventional avionics, but now for electric aircraft.

The section will continue by further supplying an overview of BLDC drive, CM voltage in power inverters, and active filter topologies. These subjects will set the base for the practical work of this study.

2.1 Issues in Electric Aircraft Related to Electromagnetic Compatibility

The increasing amount of electric hardware in more electric and all-electric aircraft (MEA and AEA) contributes to a complex electromagnetic environment, which makes electric aircraft a concern within the EMC field. Along with increasing electric hardware comes increasing wiring and reduced space. Conventional aircraft use cable bundles that must be separated to avoid crosstalk and arcing and to allow airflow between them. For compact wiring, it is necessary to add exterior shielding to avoid inter-bundle EMI [5]. In general, cable bundle placement near conductive surfaces benefits crosstalk level reduction. However, due to minimizing weight in future aircraft, composite is replacing metal body structure, and upcoming EMC issues await [6].

Replacing discrete components in inverters with integrated circuits (ICs) reduces weight and size and increases efficiency. Since weight is the main problem to overcome in future electric aircraft, ICs are making their way as leaders in this field of research. The two common IC-component motor inverters are the SiC- and GaN-based inverters. SiC (Silicon Carbide) and GaN (Gallium Nitride) semiconductors allow higher switching frequencies (compared to silicon-based semiconductors), which can reduce inverter losses but increase EMI. In a study from 2017, a comparison between an IGBT-based and SiC-based three-phase motor inverter showed motor loss improvement of the SiC inverter, but higher common-mode currents. The authors proposed that EMI filtering is crucial for inverters using wide bandgap (WBG) semiconductors such as SiC and GaN semiconductors [7].

Multilevel three-phase inverters are replacing the conventional three-phase inverter since more DC inputs can help create a smoother output voltage. Because of the multilevel inverter's harmonic reduction character and power density, suggestions of implementation in more electric- and all-electric aircraft are arising. For example, studies have shown that harmonic losses and EMI reduces remarkably with more levels in a flying capacitor multilevel inverter [8]. From an EMC aspect, recent studies have focused on CM voltage suppression in multilevel inverters. This is not an abnormality since CM issues are generally associated with inverter applications.

High-intense radiated fields (HIRF) and lightning are crucial for aircraft safety as they can induce interfering currents in avionics. Previous studies are discussing these topics within EMC in regular aircraft. Electric components are replacing mechanical hardware in electric aircraft, making the electromagnetic environment and susceptibility more complex. Thus, HIRF and lightning and their effect on avionics are worth mentioning.

A HIRF is a high-energy electromagnetic wave originating from radio and TV stations, radar emitters, and other communication infrastructures. The HIRF spectrum lies within the frequency range from 10 kHz to 40 GHz, with varying energy levels depending on the source [9]. Low-level swept current (LLSC) and low-level swept field (LLSF) are used methods for low-level HIRF testing. LLSC measures the bulk current, and LLSF is a tool for electromagnetic protection evaluation in the airframe. Shi et al. propose a step-by-step methodology of LLSC and LLSF tests on aircraft in [10]. High-level testing involves practical HIRF exposure to the aircraft and measuring the internal fields and induced currents on cable bundles [9].

Beyond the direct damage from a lightning strike on aircraft are indirect damages such as induced currents and transient voltages in the wiring [9]. Previous research on the lightning-aircraft matter is wide and has proposed many EMC-related techniques to avoid the electromagnetic harm it can cause. The extensive research on this subject has led to the ability to manage lightning strikes well in today's aircraft [11]. Thus, high-conductive materials, like metal, provide better lightning protection than lower-conductive materials (for example, different composites). However, lightning strikes have become an issue in lightweight-bodied electric aircraft due to lower material conductivity [12].

Portable electronic devices (PED) are likely to enter aircraft. In a commercial airplane, the seat average is 138 (excluding the pilot and co-pilot), and plausibly every passenger owns one or more PED like cell phones, laptops, etc.. Therefore, aircraft equipment and internal system susceptibility must be well-known to prevent interference.

The 5G network is making its way into communication devices, and cell phones utilizing the network are increasing. Analytically, 5G oper-

ational PEDs onboard may be a HIRF contributor and can potentially cause EMI in the avionics in regular aircraft [13]. The relationship between PED and HIRF, along with faster communication and increasing connection opportunities, will further complicate the electromagnetic environment in electric aircraft and predicts to become an issue in the future [14].

2.2 BLDC Motor Drive

Electric vehicles utilize BLDC motors because of their efficiency, noise characteristics, and precision instead of brushed motors, which generally are lossy and noisy. Therefore, primarily from an EMC perspective, BLDC motors are favored. An inverter enables the BLDC motor to run, where the inverter converts DC to AC by chopping up the DC with the help of transistors acting as switches. The on-and-off switching generates a pulse-width modulation (PWM) signal, which controls the output power to the electric load. This output control is also known as commutation [15]. Without rotor position sensing, the commutation will not be available for a BLDC motor because the motor windings energize sequentially. For precise rotor position sensing, BLDC motors often possess Hall sensors. The Hall sensor will output a high or low-valued signal whenever a rotor magnetic pole approaches the sensor. If the north side of the magnetic pole is nearby, the Hall sensor will output a high-valued signal, and if it is the south side passing, the output signal will be low-valued [16].

There are several commutation methods, where trapezoidal, sinusoidal, and field-oriented control (FOC) are the most prominent in the BLDC community. Depending on the desired drive characteristics, it is essential to consider the commutation method that contributes to the most efficient run. Trapezoidal control efficiently runs the BLDC motor at high frequencies but tends to generate torque ripple in the lower frequency range. Therefore, for low-speed applications, sinusoidal control is preferable. If efficient driving at low and high speeds is required, the FOC commutation is advantageous because of its wide operating frequency range. However, sinusoidal and FOC are complex methods that are time-consuming to refine and can eventually become a matter of cost-efficiency. The trapezoidal control is often favored due to its simplicity and easy implementation [17][15].

Trapezoidal commutation, also named square-wave commutation, of a three-phase BLDC motor outputs 120-degree shifted motor phase voltages. A 120-degree phase shift means that, at any moment, current conducts through any two motor windings. The phase voltage relative to the motor's neutral point will always be half the supply voltage with a 120-degree square-wave commutation. However, in reality, the phase voltage will display a more rising/falling attribute rather than a constant value of half the supply voltage, and this is due to the back EMF (BEMF) in the motor [15]. This commutation feature is shown in Fig. 1.

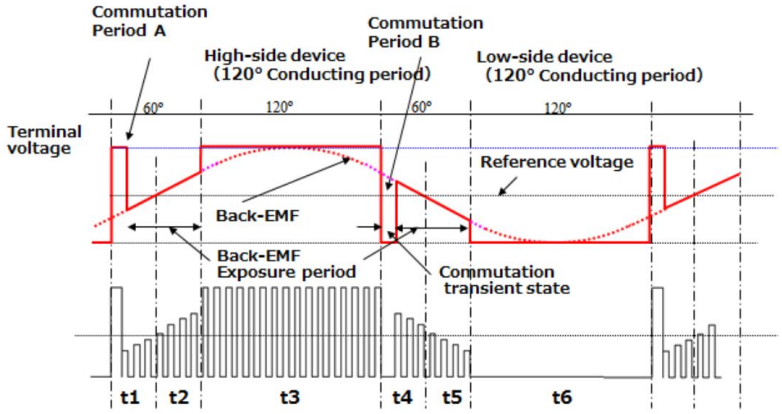

Figure 1: How 120-degree square-wave commutation appears on the motor phase voltage [15].

2.3 Common-Mode Voltage in Power Inverters

For an inverter, the CM voltage is defined as the potential voltage difference between the power source's and the load's neutral point. In a DC-fed three-phase inverter, the total CM voltage is defined as the mean of each phase voltage. The phase voltages are measured between each motor phase and common system ground [18]. The CM voltage is therefore expressed as

$$V_{CM} = \frac{V_A + V_B + V_C}{3} \tag{1}$$

where V_A, V_B and V_C denotes the motor phase voltages.

The CM current can take different paths depending on the setup. One of the main CM paths is from the inverter output back to the inverter legs. Parasitics in the motor cables allow CM current to couple to the system ground and conduct back to the inverter leg via the DC link. Another CM path is via the (grounded) motor housing and back to the power supply, which generates a larger CM loop area. The latter is generally known to cause bearing failures in the motor [19].

2.4 Motor Drives with Active Filters

An active EMI filter is an electronic circuit built with active components intended for EMI suppression. Feedforward and feedback are the two main typologies of active filters. The feedforward filter injects a predicted destructive interference, and the feedback filter measures the noise and injects an anti-noise signal. The correct placement of both typologies is

between the noise source and the load. The feedforward filter injects the predicted signal at the load, and the feedback filter measures the load noise and injects the filter output at the source [20].

In electric motor inverters, the CM noise source is the fast-switching elements of the inverter legs. The high $\frac{dv}{dt}$ causes parasitic capacitors between the motor phase windings and the motor frame to conduct, which induces inevitable CM currents in the ground plane [21]. The charging and discharging of the parasitics produce current spikes that, via ground, conduct back to the noise source, i.e., the motor inverter. A basic idea of an active CM cancellation filter applied to a single-phase inverter is shown in Fig. 2. A cancellation inverter leg is applied across the original motor inverter leg. Its purpose is to generate an anti-inverter signal, thus generating an anti-CM signal. The output of the cancellation inverter leg is connected via a cancellation capacitor to the motor housing. Due to the cancellation capacitor, the CM current is only allowed to loop between the inverter, motor, and cancellation inverter. The cancellation inverter is recommended to have the same supply voltage as the original inverter leg. For a three-phase inverter, a three-phase cancellation inverter is needed. However, for three-phase space vector modulation (SVM) drive, two cancellation inverter legs are sufficient. Depending on the PWM method, the CM cancellation filter can be optimized to two phases for a three-phase system [22].

Fig. 3, shows applications of an active CM EMI filter (ACEF) circuit, based on current sensing and compensation. The CM choke, L_{CM}, intends to measure the CM current. When high-frequency current conducts through the windings, the choke will generate a high-frequency flux that produces a high-frequency voltage at the input terminal of the transconductance amplifier. C_0 is used for current injection to ground. C_c is necessary for closing the loop of the filter and provides a low-impedance path of the high-frequency CM current, allowing the current to circle the loop. V_c is the filter bias voltage for the amplifier and at low frequencies, C_c's impedance will be large enough to isolate the bias voltage from the main voltage [23]. Designs of active CM cancellation filters have been limited to conducted EMI up to several MHz. The before-seen filter techniques are not sufficient for suppressing radiated emissions above 30 MHz. An active CM cancellation filter, shown in Fig. 4, and an active CM filter, shown in Fig. 5, can be combined to achieve radiated emissions suppression for higher frequencies. The overall concept of the presented active CM canceller is to achieve CM voltage, v_{cmo}, cancellation by injecting a compensating voltage, v_{acc}. The active CM filter is a combination of a high-frequency passive filter and a feedback voltage-sensing parallel-compensating (VSPC) active filter, this part includes a compensating capacitor, C_{comp}, a sensing capacitor, C_{sense}, and a voltage-feedback circuit. The sensing network forms a high-pass filter circuit for reducing unwanted low-frequency and high-amplitude CM voltage components. The operational amplifier completes

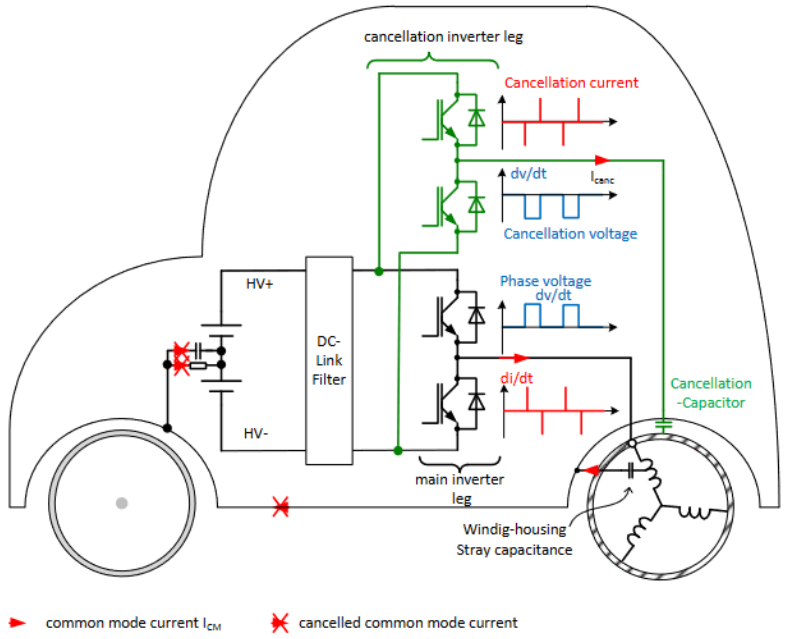

Figure 2: Schematic of the main inverter leg and cancellation inverter leg. A cancellation capacitor connects the output of the cancellation inverter leg to the motor housing. Red arrows are the remaining CM currents and crossed-out red arrows are the canceled CM currents [22].

the voltage-feedback circuit and will sense the CM voltage between the power cable and ground and feeds the voltage to C_{comp}. This compensation will suppress radiation noise from the power cable [24].

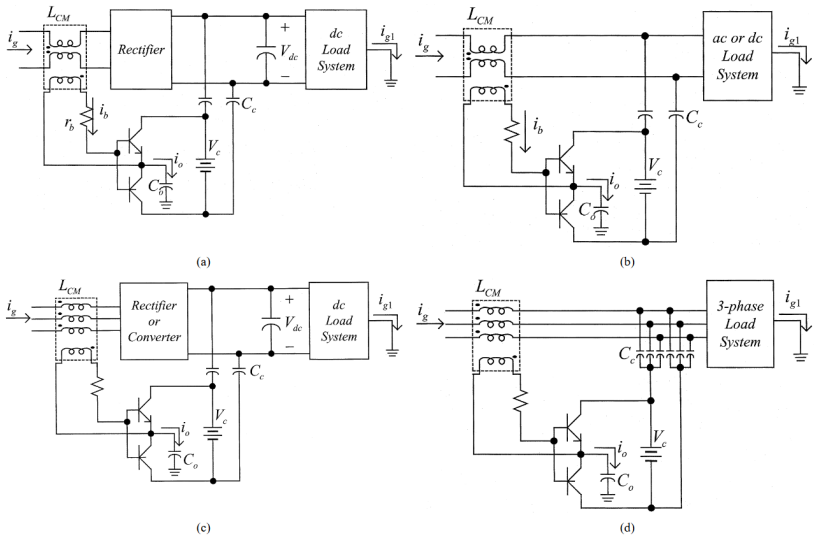

Figure 3: Configurations of proposed ACEF: (a) ACEF with DC-bus coupling (single-phase inverter), (b) ACEF with AC line coupling (single-phase inverter), (c) ACEF with DC-bus coupling (three-phase inverter), and (d) ACEF using AC line coupling (three-phase inverter) [23].

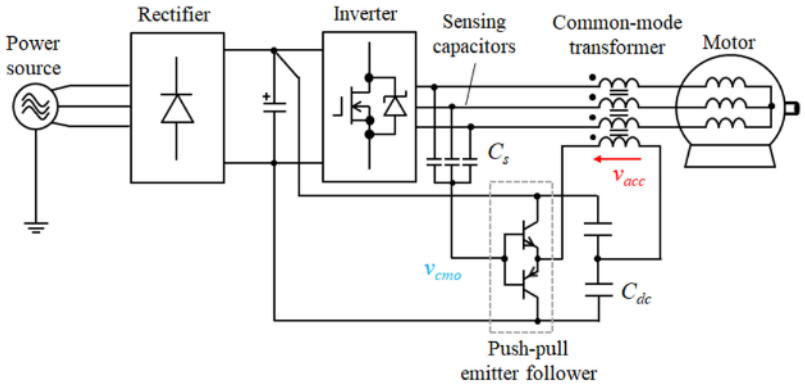

Figure 4: Active CM cancellation filter applied to a three-phase inverter and motor [24].

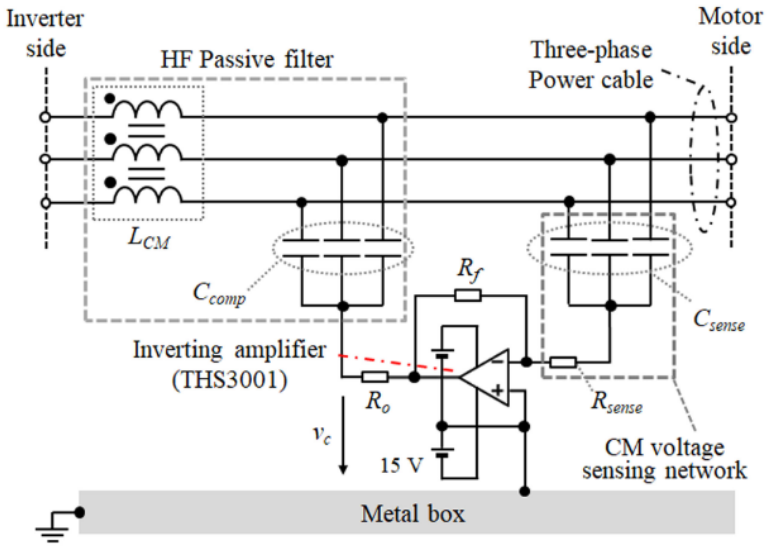

Figure 5: Schematics of the active CM filter connected to a three-phase power cable [24].

The design of the active EMI filter generally incorporates three main building blocks: a sensing circuit, signal manipulation with active components, and an injection circuit. As seen in Fig. 3, a CM choke and resistors in series are optional for sensing CM currents, and in Fig. 4-5, a capacitor-resistor network senses CM voltages. There are two different injecting methods, capacitors for current injection, as seen in Fig. 2, 3 and 5, and a (three-phase) transformer for voltage injection, shown in Fig. 4. The active part can be constructed with transistors, as in [23] and [25], or an operational amplifier, as [24] suggests. However, [22] proposes an inverted inverter for active current cancellation, which differs from the traditional active EMI filter designs that [23], [25], and [24] present.

3 Method

3.1 Cypress Motor Kit

The Cypress motor kit, shown in Fig. 6, is programmed to run a 120-degree square-wave commutation on a three-phase BLDC motor. The motor inverter is a MOSFET dual H-bridge with four half-bridges in total. Fig. 7 shows the motor inverter where the three leftmost half-bridges drive the three motor phases, A, B, and C [16]. The BLDC motor is an eight-poled BLY172S-24V-4000 produced by Anaheim Automation. The motor has a star connection configuration and three Hall sensors [26]. A battery pack with two 12 V lead-acid battery banks with a series connection supplies the motor kit with 24 V.

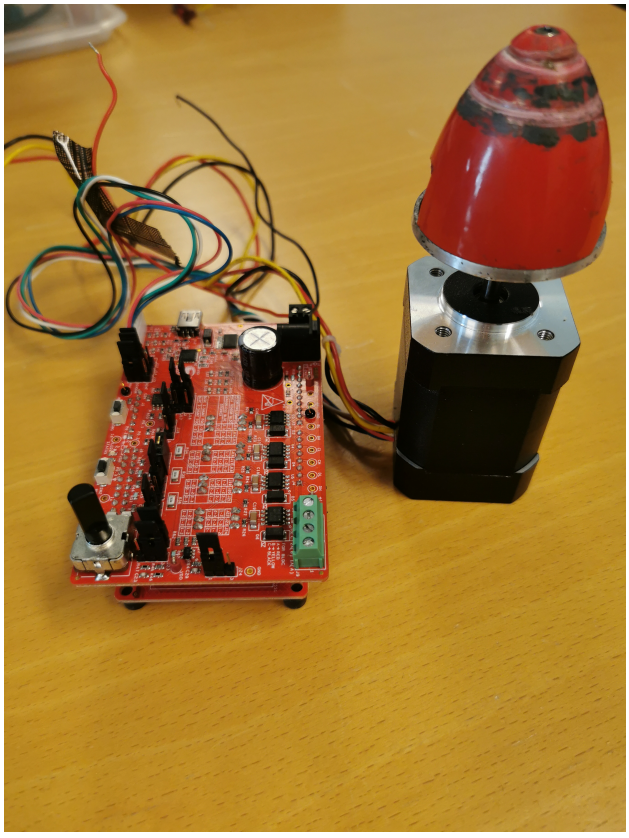

Figure 6: The Cypress motor kit. To the left is the motor control evaluation board and to the right is the BLY172S-24V-4000 BLDC motor.

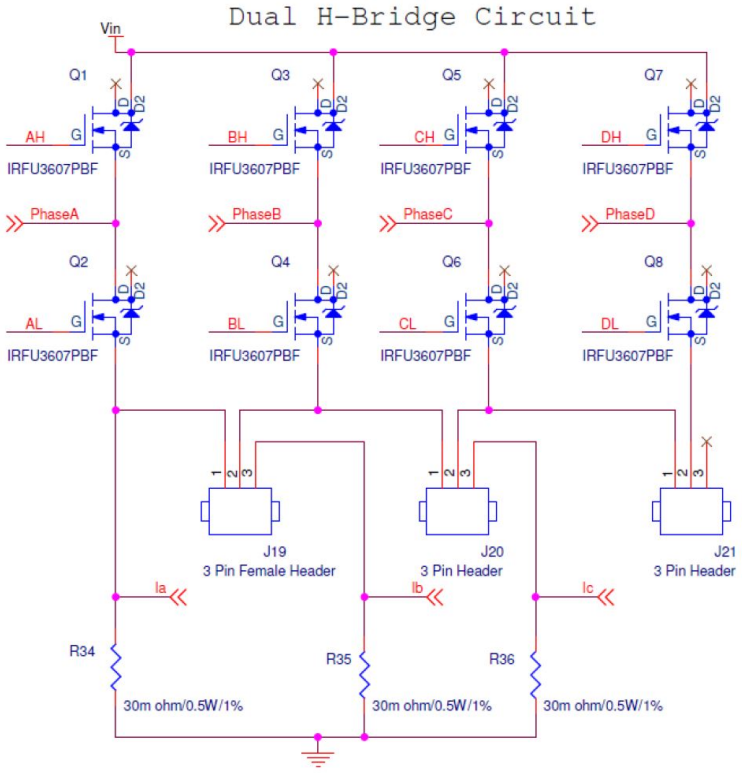

Figure 7: Dual H-bridge circuit for driving the motor. Every inverter leg is a half H-bridge circuit with an upper and lower IRFU3607PBF MOSFET. The gates of the MOSFETs are driven by a dual H-bridge driver [16].

The motor phase voltages are measured directly at the inverter output with 500 MHz probes. The waveforms are displayed on and saved from a four-channel RBT2004 Rohde & Schwartz oscilloscope. The saved data is then handled and manipulated in Matlab. Motor phase voltage A, B and C are displayed in Fig. 8. The Hall sensor voltages are measured by connecting the probes at the Hall sensor output. The Hall sensor voltages are shown in Fig. 9. The period time of the Hall voltages is approximately 3.8 ms and the amount of time it takes the eight-poled motor to rotate one revolution is

$$1 \text{ Revolution} = T_{Hall} \cdot \textit{(No. pole pairs)} = (3.8 \cdot 10^{-3}) \cdot 4 = 15.2 \cdot 10^{-3} \text{ s}, \quad (2)$$

which is equivalent to ca 66 Hz and corresponds to 3950 RPM.

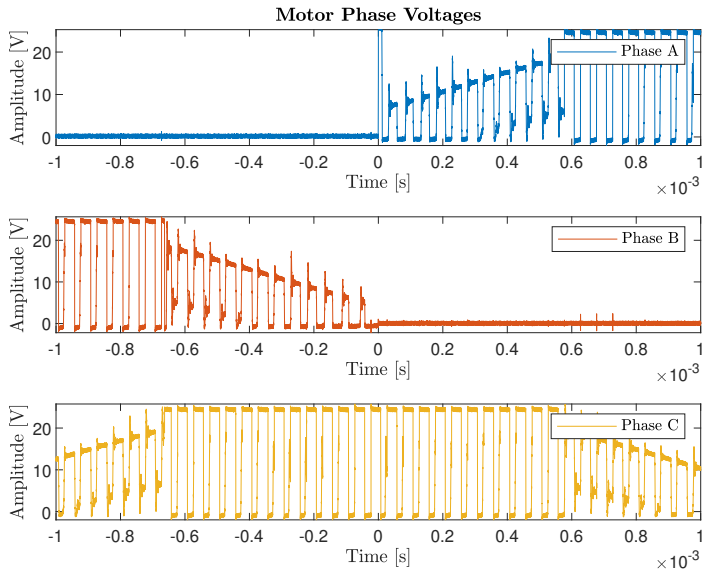

Figure 8: Measured motor phase voltages of phase A, B and C.

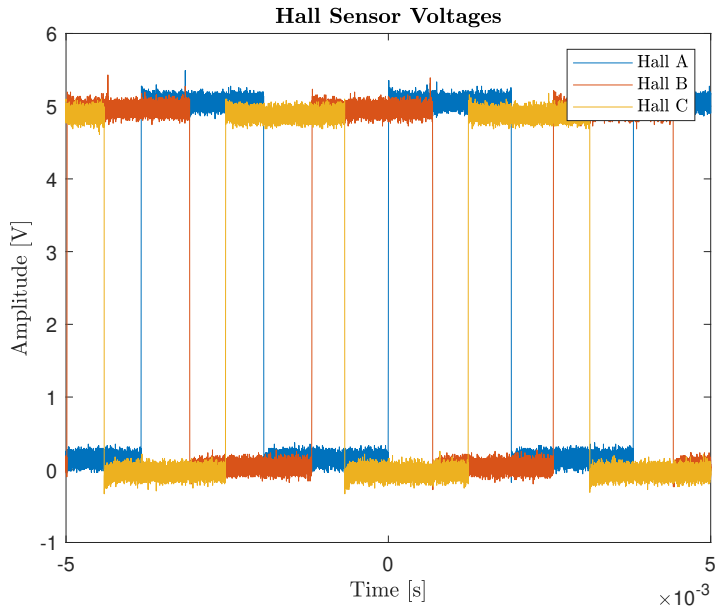

Figure 9: Measured Hall voltages of phase A, B and C.

3.1.1 Parasitics Model

In Fig. 10, the ringings on a motor phase are zoomed in. The ringings were discovered during the measurements and are somewhat of a side trail to this study. The ringing appears in the state when the BEMF exposes itself in the motor phase, as mentioned in Section 2.2. The ringing frequency is calculated from the data as

$$f_{ringing} = \frac{1}{T_{ringing}} = \frac{1}{5.46\ \mu\text{s}} \approx 180\ \text{kHz}. \tag{3}$$

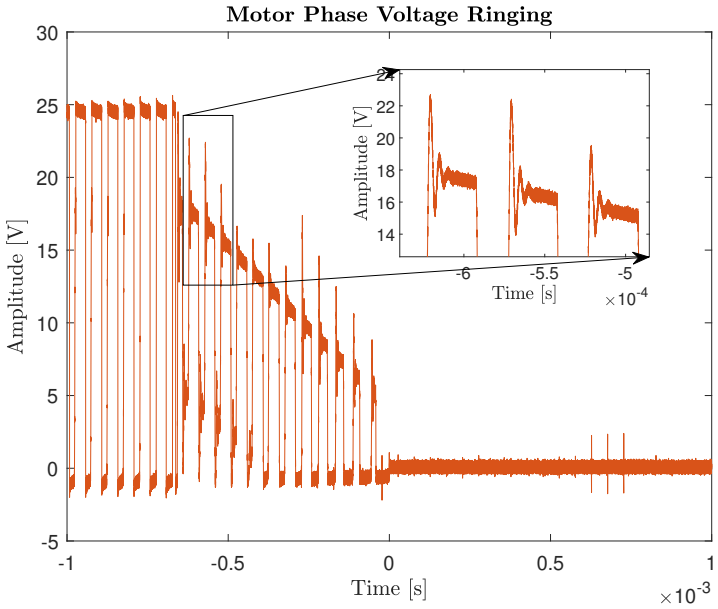

Figure 10: Ringings on the motor phase under the period of time when the phase is affected by the BEMF of the motor.

The state is modeled in Orcad PSpice to understand the origin of the ringings. Whenever the BEMF affects a motor phase, the two respective motor phases will be low and high, and Fig. 8 confirms this trend. For example, in the period 0-0.6 ms, the BEMF influences phase A, phase B is low, and phase C is high, implying that the pulse source drives C, phase B is grounded, and the current path for phase A is through the lower inverter leg MOSFET. The schematic of this model is shown in Fig. 11. Since the half-bridge corresponding to phase A is not conducting, the MOSFETs are off. Therefore, the gate of the lower transistor is at ground potential.

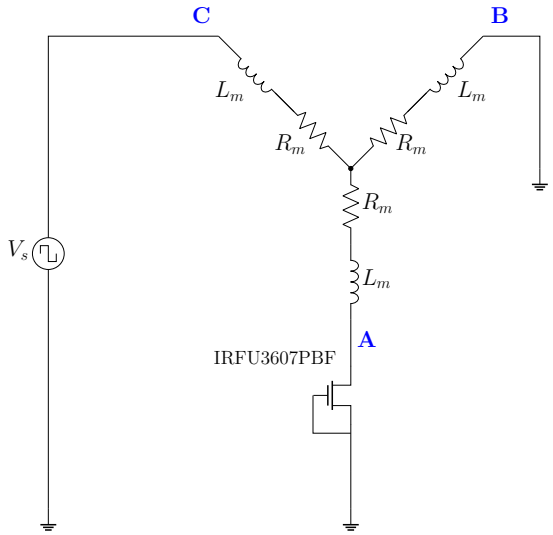

Figure 11: Circuit model of the state when the motor phase is exposed to BEMF. However, the actual BEMF itself is not included in the model. The pulse voltage source, V_s, replicates the PWM signal on motor phase C, the motor phase B is grounded, and motor phase A is connected to the switched-off lower inverter MOSFET. The motor inductance and resistance are denoted L_m and R_m.

Ringings may occur as a resonance between the parasitic coil capacitances and the coil itself, called self-resonance. However, if the ringings were due to the motor winding's self-resonance, ringings would appear everywhere on the motor phase voltage waveform.

Whenever the motor phase is high or low, the low-impedance path will "cling" the motor phase. When the motor phase goes from high to low, the phase is connected to the off-switched inverter leg MOSFETs, which makes a high-impedance phase output node. In this state, nothing holds on to the motor phase and it appears to float, which allows oscillations to occur on the line. This speaks for that the ringings might be a resonance between the motor winding and parasitic drain-source capacitance, C_{ds}, of the MOSFET.

Placing resistors parallel to the windings will dampen the ringings because it will increase the damping factor of the RLC system's step response [27]. The line-to-line damping resistors, R_d, are shown in the schematic in Fig. 12.

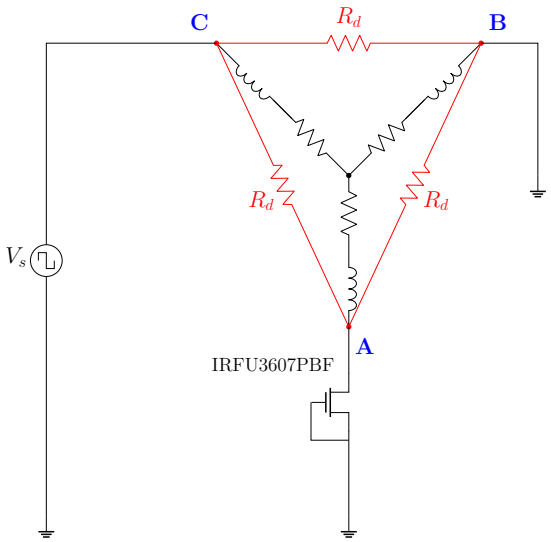

Figure 12: Same circuit model as in Fig. 11, but with added damping line-to-line resistors, R_d.

The circuits presented in Fig. 11-12 are simulated in Orcad PSpice and Table 1 lists the component values used in simulations. The motor resistance and inductance are motor specifications from [28]. The motor phase will ideally be at half supply potential when not including the BEMF, as stated earlier in Section 2.2. Simulation results confirm the statement in Fig. 13. The ringings in the simulation are measured in Orcad to be approximately 150 kHz, which is a slightly lower frequency than the ringings on the motor phase voltage. Simulations show that the damping resistors nearly eliminate the ringings occurring when the phase is neither high nor low. When constructing the damping circuit, the damping resistors will be two 1 kΩ resistors in parallel to enable more power dissipation.

Table 1: Component values in the models in Fig. 11-12 for simulation and testing.

Component	Description	Value
V_s	Pulse source	$A = 24$ V, $f = 20$ kHz
L_m	Motor inductance	1.2 mH
R_m	Motor resistance	0.8 Ω
R_d	Damping resistor	500 Ω
C_{ds}	Parasitic drain-source capacitance of IRFU3607PBF [29]	360 pF

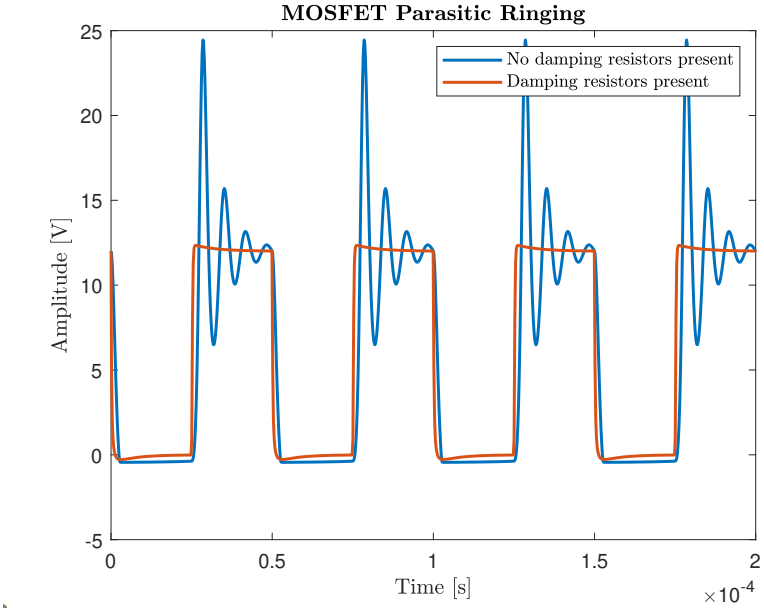

Figure 13: Simulation results of the damped ringings caused by parasitic capacitances in the MOSFETs of the inverter legs.

3.2 Active Cancellation Filter

Fig. 14 proposes a design of an ACF. A voltage pulse source, V_s, supplies the circuit, and the model includes its resistance, R_s. C_1 and R_1 in the inverting terminal of the operational amplifier is a sensing network. The

sensing network is a high-pass RC filter with a cutoff frequency of

$$f_{HP,cf} = \frac{1}{2\pi RC}. \tag{4}$$

The sensed signal enters a high-speed inverting OP-amp, THS3121, where the feedback resistor R_2 sets the gain together with R_1 as

$$G = -\frac{R_2}{R_1}. \tag{5}$$

The OP-amp inverts the signal and generates an anti-signal. The OP-amp's output resistor is kept small and prevents the OP-amp from oscillating. The transformer acts as a voltage injector which injects and adds the anti-signal to the source signal and eventually cancels it.

An LCR meter is used to measure the actual stray capacitance between the shorted motor phases and the housing at several frequencies between 1 kHz-200 kHz. The capacitive load, C_L, reflects this stray capacitance between the motor windings and housing.

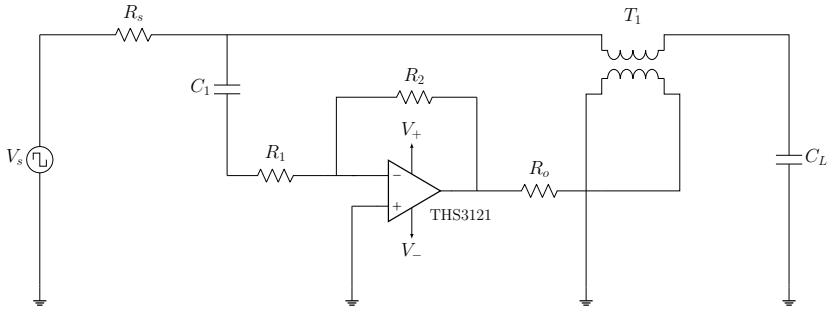

Figure 14: Proposed ACF circuit.

3.2.1 Transformer

The core of the transformer is a B66367GX187 ungapped ferrite E-core. The E-cores are placed in a former and are firmly pressed against each other to avoid gapping between them. The number of wire turns around the former is dependent on the characteristics and geometry of the E-core. The desired self-inductance, L in H, is calculated as

$$L = A_L N^2 \tag{6}$$

where A_L is the core's inductance coefficient and N is the number of turns of wire around the coil [30]. From the datasheet [31] of B66367GX187 the typical value of A_L is 3800 nH. Using Eq. 6 with $N = 60$ turns, yields approximately 13 mH self-inductance of the coil. To inject the anti-signal into the motor phase voltage, as high as possible inductance is desired. Because of the size of the coil, only 60 turns fit on the former.

3.2.2 Simulations

The ACF is simulated in Orcad PSpice, and Fig. 15 shows the simulation result with the component values listed in Table 2. The blue graph in the simulation result is the pulse source, and the red graph illustrates the signal measured at the capacitive load, C_L. The cancelled signal has a slanting appearance due to the voltage drop across the output resistor, R_o. The Fourier transform of the source signal and the cancelled signal is depicted in Fig. 16. As the spectrum indicates, the proposed ACF successfully suppresses harmonics and noise up to 2 MHz. After 2 MHz, the spectrum of both signals converges toward each other, which means that the filter performance is insufficient at higher frequencies.

Table 2: Component values for the proposed ACF.

Component	**Description**	**Value**
V_s	Pulse source	$A = 5$ V, $f = 20$ kHz
R_s	Source resistance	50 Ω
C_1	Sensing network capacitance	100 μF
R_1	Sensing network resistor/ inverting input resistor	1 kΩ
R_2	Feedback resistor	1 kΩ
R_o	Output resistor	10 Ω
T_1	Transformer (primary and secondary winding)	13 mH
C_L	Capacitive load	130 pF

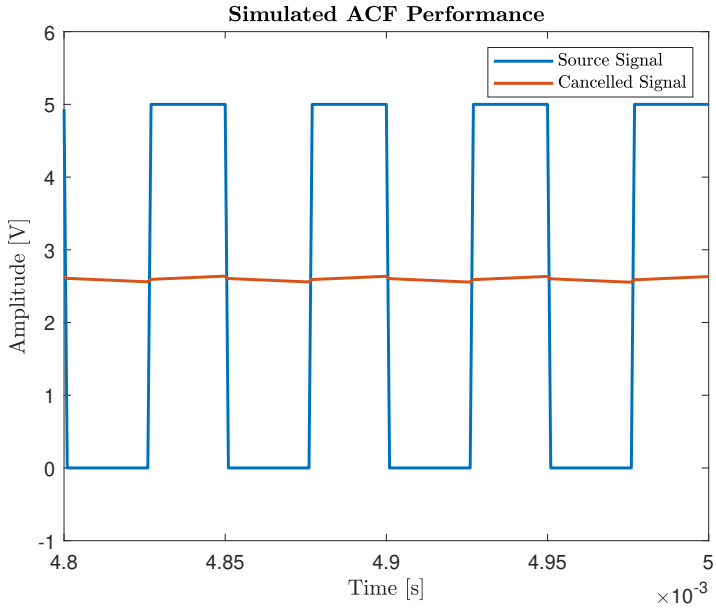

Figure 15: Simulated result of the proposed ACF.

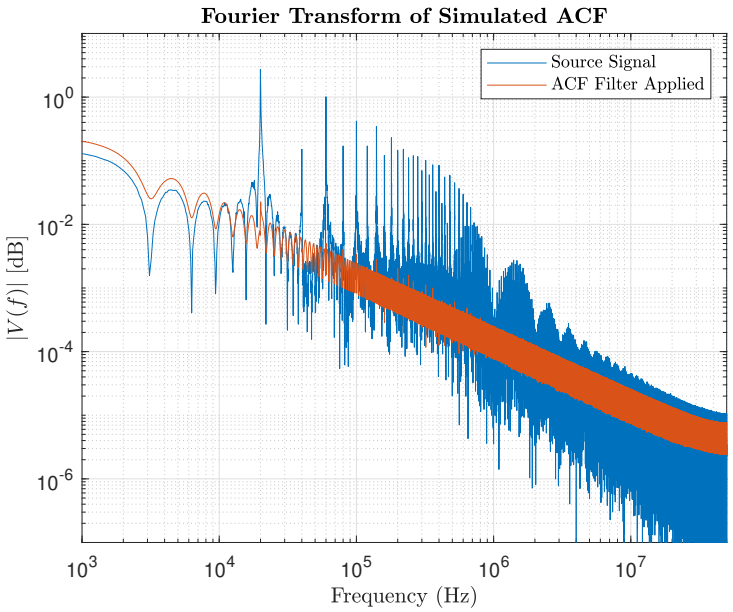

Figure 16: Fourier transform of the simulated result of the proposed ACF.

3.3 Hybrid Filter

The hybrid filter is a mix of an active and a passive filter. It consists of the proposed ACF with a passive part add-on. Fig. 17 displays the proposed hybrid filter, where the red part is the passive element in the filter. The ACF performs well up to a few MHz, and the purpose of the added passive filter is to increase attenuation at the higher frequencies.

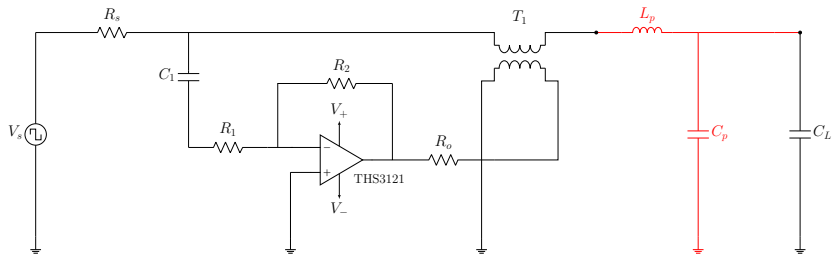

Figure 17: Proposed hybrid filter.

3.3.1 Simulations

The passive filter component values are listed in red in Table 3, and its cutoff frequency is

$$f_{LC,cf} = \frac{1}{2\pi\sqrt{LC}} = \frac{1}{2\pi \sqrt{(68 \cdot 10^{-6}\ \text{H}) \cdot (470 \cdot 10^{-12}\ \text{F})}} \approx 0.9\ \text{MHz}, \tag{7}$$

and will be enough to cover the desired frequencies. Fig. 18 depicts the Fourier transform of the simulation result of the hybrid filter. The blue spectrum illustrates the pulse voltage source, V_s, and the red spectrum is the hybrid filter when applied to the source. The peak at ca 1 MHz portrays the filter cutoff frequency. Beyond this frequency, a drop is expected but does not occur. Simulations confirm that the added passive part does not contribute to noise suppression.

Table 3: Component values for the hybrid filter.

Component	**Description**	**Value**
V_s	Pulse source	$A = 5$ V, $f = 20$ kHz
R_s	Source resistance	50 Ω
C_1	Sensing network capacitance	100 μF
R_1	Sensing network resistor/ inverting input resistor	1 kΩ
R_2	Feedback resistor	1 kΩ
R_o	Output resistor	10 Ω
T_1	Transformer (primary and secondary winding)	13 mH
C_L	Capacitive load	130 pF
L_p	Inductor in passive filter	68 μH
C_p	Capacitor in passive filter	470 pF

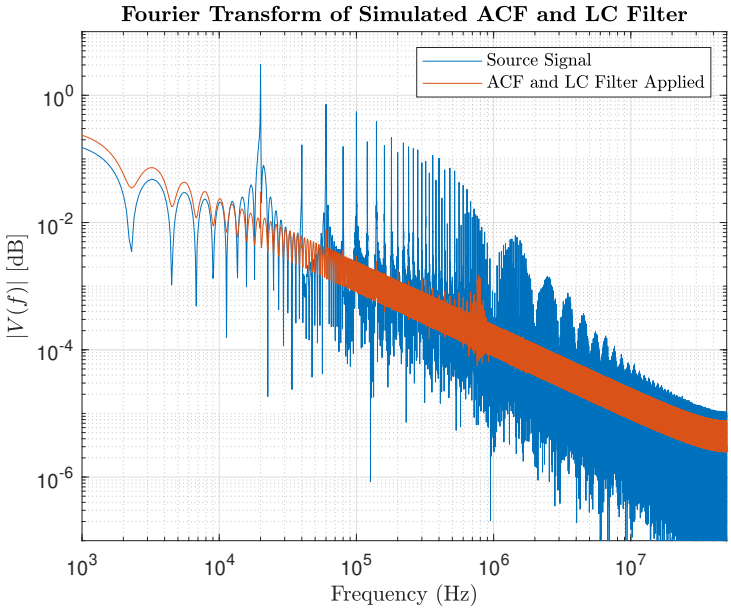

Figure 18: Fourier transform of the simulated result of the proposed hybrid filter.

4 Results

4.1 Motor Drive

The CM voltage is evaluated according to Eq. 1, where the motor phase potentials are measured relative to ground. The CM voltage in the system is depicted in Fig. 19, where the amplitude reaches as high as 17 V. Fig. 20 displays the Fourier transform of the CM voltage, which is similar to the Fourier spectrum of the motor phase voltages, as seen in Fig. 21. The peak at 20 kHz is the fundamental frequency and originates from the PWM frequency of the motor inverter. The additional peaks through the spectrum are harmonics of the fundamental frequency.

The noise source of the harmonics at higher frequencies, just below the GHz range, is challenging to evaluate and may emerge from any of the electronic components on the Cypress motor board.

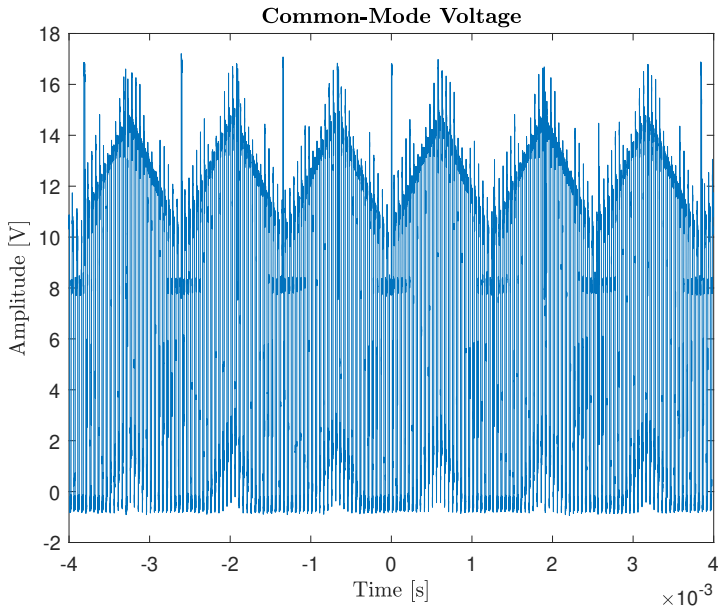

Figure 19: Measured CM voltage of the Cypress motor kit.

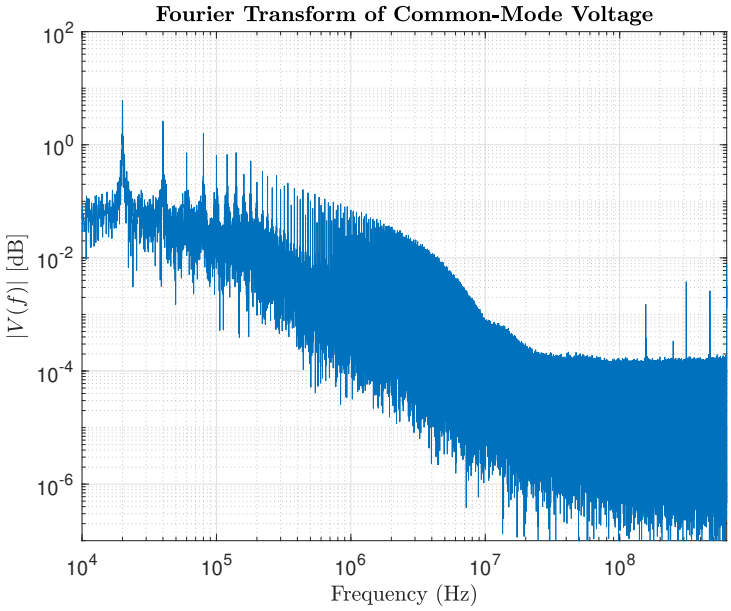

Figure 20: Fourier transform of the CM voltage.

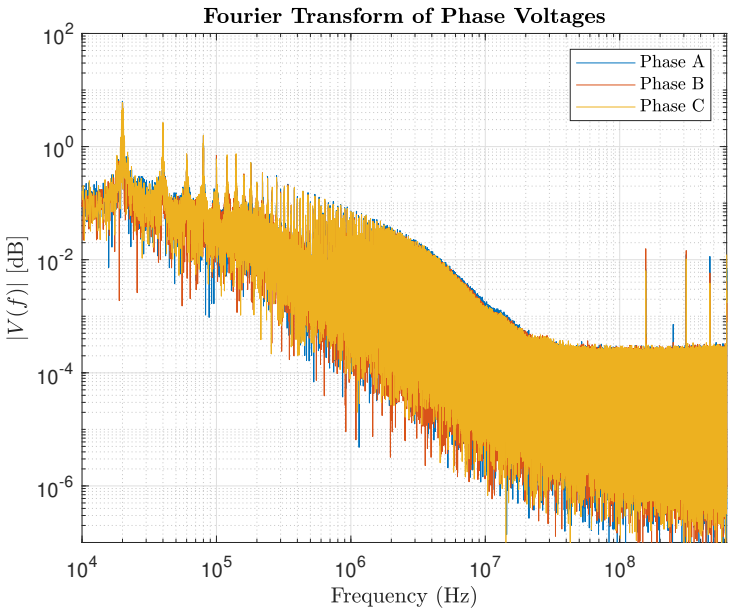

Figure 21: Fourier transform of the motor phase voltages.

4.1.1 MOSFET Parasitics

Simulation has confirmed that damping resistors added line-to-line dampens the ringing frequencies that the motor windings and parasitic MOSFET drain-source capacitance cause. When damping resistors are mounted onto the in-real-life system, it nearly eliminates the ringing frequencies occurring in the state when the BEMF in the motor inflicts the motor phase, as seen in Fig. 22.

Fig. 23 illustrates the Fourier transform of the motor phase voltages when damping resistors are included. The damping resistors slightly decrease the noise floor between 100 kHz-1 MHz, compared to the spectrum of the motor phase voltages in Fig. 21.

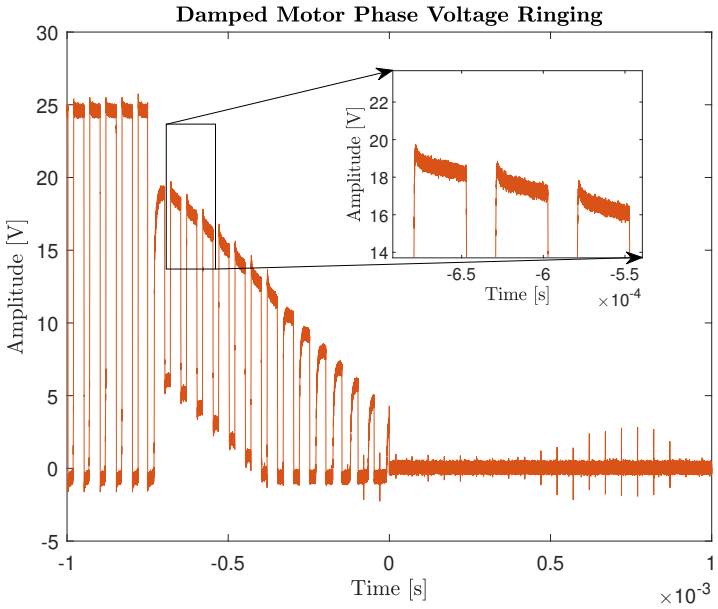

Figure 22: Measured motor phase voltages with the damping resistors.

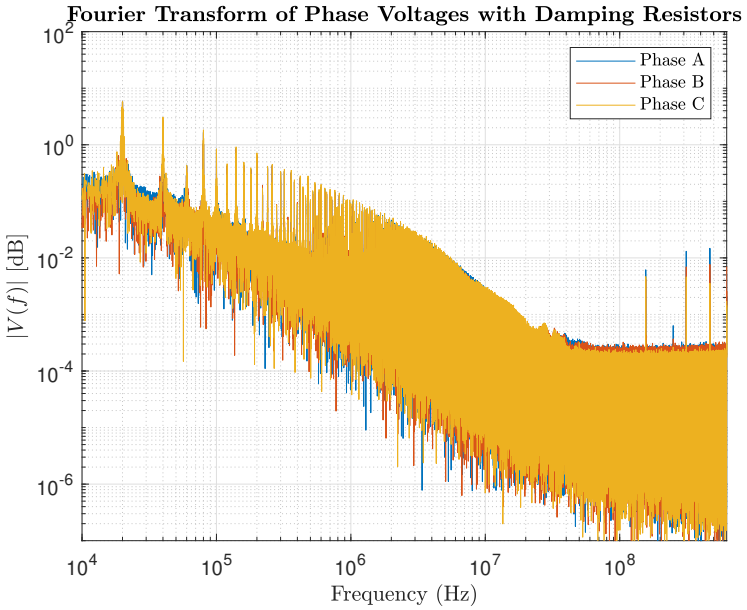

Figure 23: Fourier transform of the motor phase voltages with damping resistors.

4.2 Active Cancellation Filter

Fig. 24 shows the measured data from the constructed ACF that Fig. 25 displays. The slanting appearance in the cancelled signal from simulations was also visible in the measurements. However, tuning the gain on the OP-Amp by placing a potentiometer in series with the feedback resistor, R_2, solved the issue.

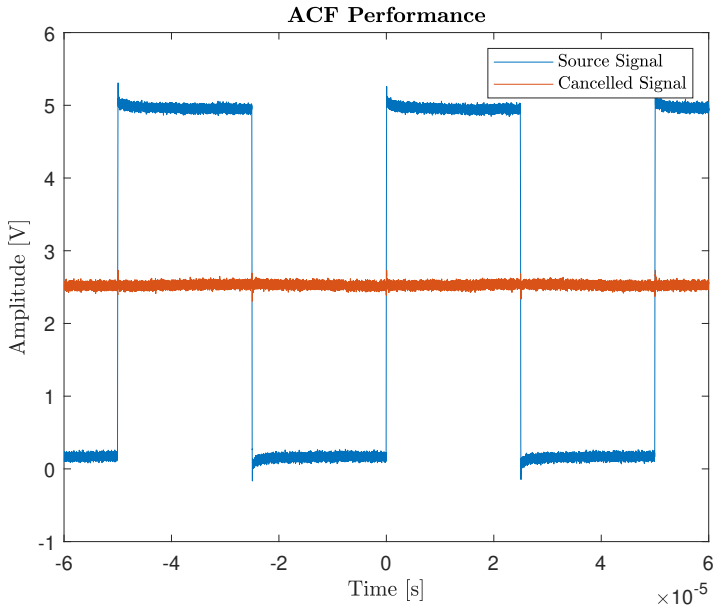

Figure 24: ACF performance measurement.

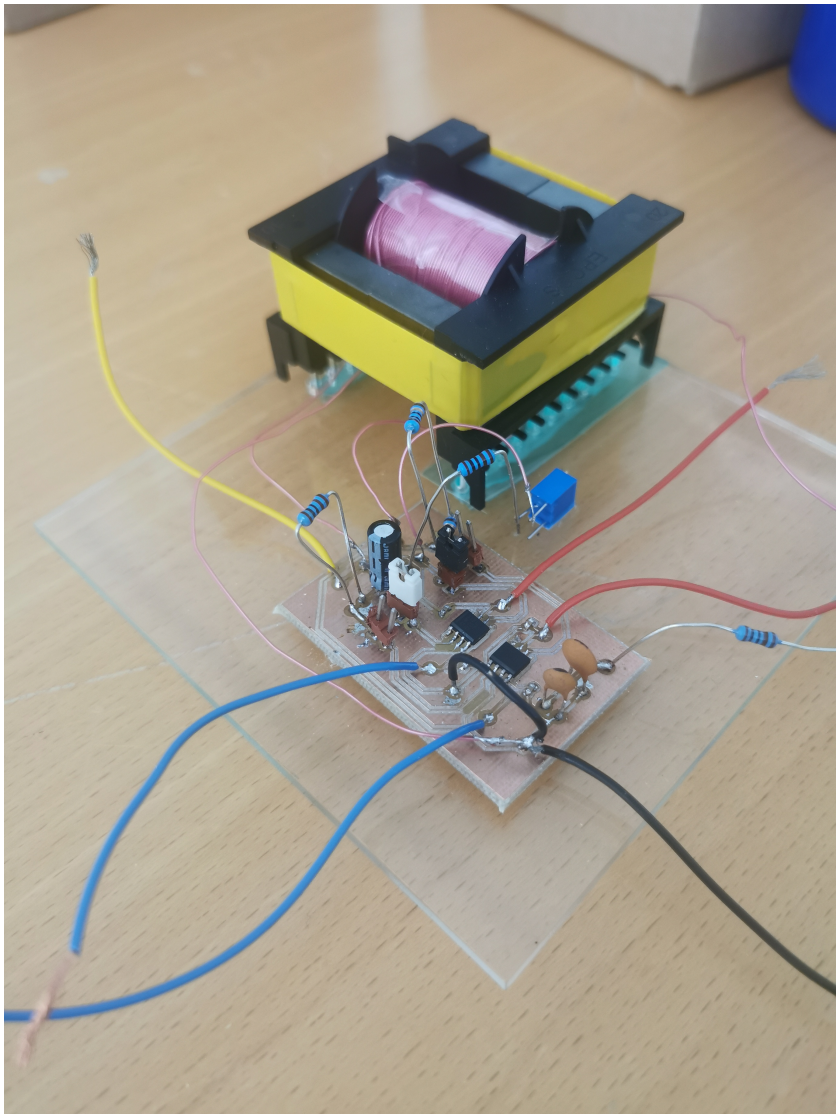

Figure 25: Constructed ACF. The device with the pink windings is the transformer where the voltage injection to the motor phase occurs.

The Fourier transform of the ACF performance, in Fig. 26, shows a harmonic cancellation that reaches up to 10 MHz. At 100 MHz, the spectrum of the source and cancelled signal converges to the oscilloscope's noise floor. The filter suppression will never reach below the noise floor, indicating that measurements with the RBT2004 oscilloscope limit measurement of filtering results at frequencies this high.

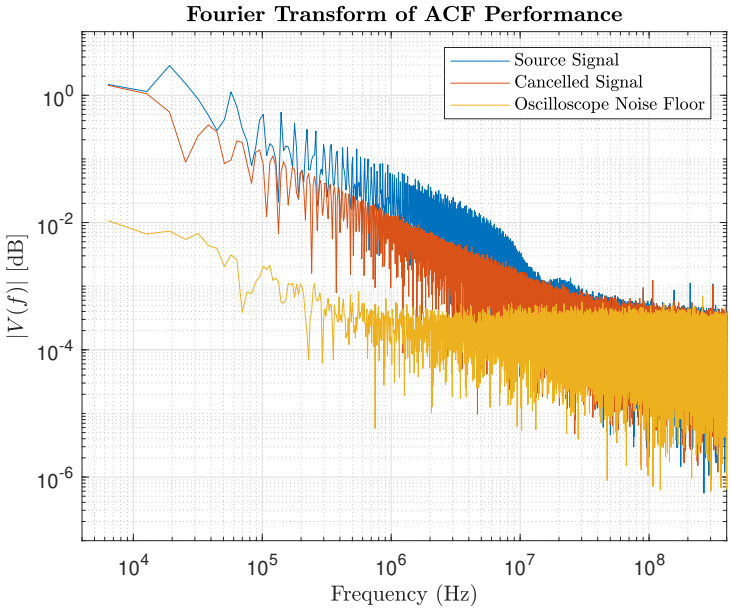

Figure 26: Fourier transform of the ACF performance. The blue spectrum is the source signal, the red spectrum is the cancelled signal and the yellow is the noise floor of the oscilloscope.

4.3 Hybrid Filter

The passive part of the hybrid filter is initially solely connected to the source signal, and its Fourier spectrum is shown in Fig. 27. The peak at just below 1 MHz in the cancelled signal originates from the filter cutoff frequency, and the filter suppresses the source signal up to 10 MHz. As for the ACF, the LC filter fails to suppress noise at 10-100 MHz, whereafter the signal spectra hit the noise floor.

Fig. 28 displays when both the passive filter and ACF are connected to the voltage pulse source. The spectra are no further different from the spectra in Fig. 26. The passive filter is ineffectual, which simulation results from the hybrid filter have shown earlier in Fig. 18.

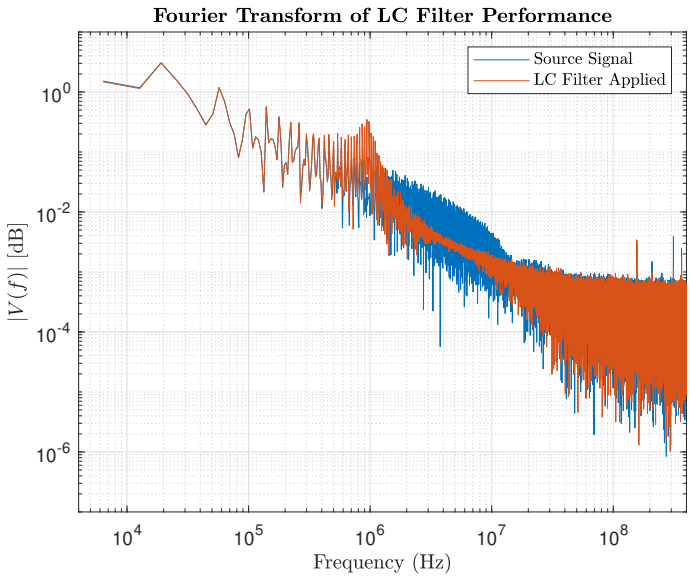

Figure 27: Fourier transform of LC filter performance. The blue spectrum is the source signal and the red spectrum is when only the LC filter is applied to the source.

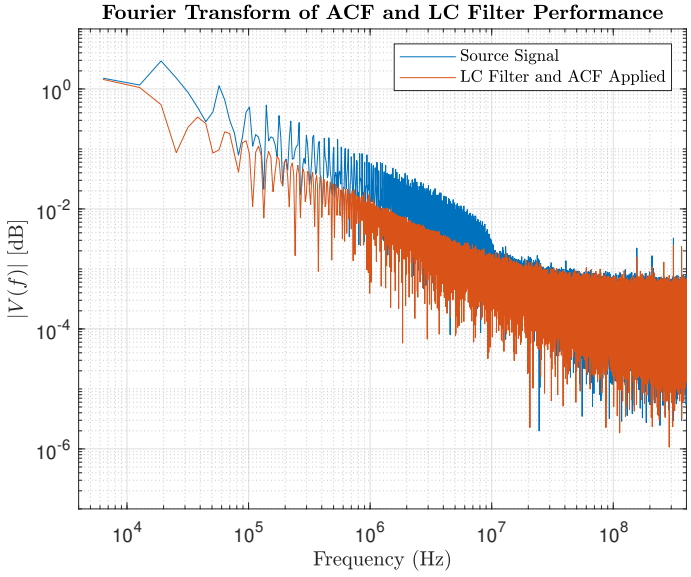

Figure 28: Fourier transform of the hybrid filter performance. The blue spectrum is the source signal and the red spectrum is when both the ACF and the LC filter are applied to the source.

5 Discussion

The electrification of vehicles makes a central point in today's environmental debates. Electric aircraft is significant in reaching global sustainable development goals, and research is advancing. The electronic environment in electric aircraft has become a subject of matter in the EMC field. The electric drive systems are noisy due to high switching rates, and filtering must be acquired to prevent interference within and from the aircraft.

Damping resistors are a typical method of suppressing ringing frequencies. However, applying damping resistors line-to-line on a three-phase BLDC will load the system more than necessary and reduce efficiency. The knowledge of the lower inverter leg MOSFET parasitic's impact on the system is more relevant than the damping method. The information gives an insight into the noise source and is convenient for future ACF motor applications. Afterward, it was discovered that the parasitics model is missing the upper inverter leg MOSFET, which will contribute to the total output capacitance of the inverter leg. This may be why the measured ringing frequency on the motor phase was 180 kHz, compared to the simulated ringings which had a frequency of only 150 kHz.

The ACF and hybrid filter's inability to suppress noise between 10 MHz to 100 MHz is notable. A hardware problem is most unlikely when the same filter behavior appears from simulated results. Another explanation may be due to spectral leakage or spectral resolution issues. Window functions and zero padding are tools that prevent Fourier transform problems similar to these.

The upcoming near-future task is to dimension the ACF to make it applicable to the Cypress motor kit. The future goal is to propose a high-voltage ACF implementation for electric aircraft. Researchers raise the issue of considering weight, which makes integrated electronic solutions attractive. Therefore, an IC ACF will be proposed to ensure weight minimization, but not in the near future.

6 Conclusion

This study has provided a deep understanding of the EMC/EMI challenges with electric aircraft, where electric propulsion and active canceling filter targeting electric aircraft has been in focus.

Three-phase BLDC motors have been studied and tested from an EMC point-of-view. Parasitic capacitances of the lower MOSFETs in the inverter legs, that were causing ringings on the motor phase voltages, were observed. The ringings can be dampened by applying damping resistors line-to-line, though this is not the most optimal solution for the problem. The knowledge of the parasitic capacitance influence on the motor is relevant for future tests with the Cypress motor kit.

This study proposed a single-phase ACF and hybrid filter for the purpose of eliminating harmonics from a square-wave pulse generator. The ACF was expecting to target the harmonic suppression at frequencies up to a few MHz. The passive LC filter add-on in the hybrid filter was supposed to cover the higher frequency band, where the ACF was unable to operate sufficiently. The ACF worked as intended and suppressed harmonics from a pulse generator up to 10 MHz, and the hybrid filter was designed to have a cut-off frequency at around 1 MHz but showed no impact in simulations or measured results. However, the observed results may be caused by software issues, where more sophisticated Fourier transform methods are required.

The studied subjects of this thesis will act as a fundament for future work within electric propulsion and ACF targeting electric aircraft. It is early to conclude whether the ACF proposed is suitable for implementation on an electric aircraft. Therefore, at this moment, it is not possible to say if this filtering technique will suppress the harmonic noise of power inverters in electric aircraft.

References

[1] European Commission. *Reducing emissions from aviation*. URL: https://climate.ec.europa.eu/eu-action/transport-emissions/reducing-emissions-aviation_en. (Accessed: 2023-05-11).

[2] European Commission. *Electrification of the Transport System*. Directorate - General for Research, Innovation - Smart, Green, and Integrated Transport, 2017.

[3] Casey Crownhart. *This is what's keeping electric planes from taking off*. URL: https://www.technologyreview.com/2022/08/17/1058013/electric-planes-taking-off-challenges/t/. (Accessed: 2023-01-27).

[4] Heart Aerospace. *Learn more about the ES-30*. URL: https://heartaerospace.com/es-30/. (Accessed: 2023-01-27).

[5] Jesper Lansink Rotgerink et al. "EMC aspects of compact wiring for future aircraft". In: *2018 IEEE International Symposium on Electromagnetic Compatibility and 2018 IEEE Asia-Pacific Symposium on Electromagnetic Compatibility (EMC/APEMC)*. 2018, pp. 165–170. DOI: 10.1109/ISEMC.2018.8393760.

[6] Jesper Lansink Rotgerink, Ramiro Serra, and Frank Leferink. "Multiconductor Transmission Line Modeling of Crosstalk Between Cables in the Presence of Composite Ground Planes". In: *IEEE Transactions on Electromagnetic Compatibility* 63.4 (2021), pp. 1231–1239. DOI: 10.1109/TEMC.2020.3040689.

[7] Victor Dos Santos et al. "Trade-off between losses and EMI issues in three-phase SiC inverters for aircraft applications". In: *2017 IEEE International Symposium on Electromagnetic Compatibility & Signal/Power Integrity (EMCSI)*. 2017, pp. 55–60. DOI: 10.1109/ISEMC.2017.8077991.

[8] Anudari Tumurbaatar et al. "Harmonic Loss Reduction in High Speed Motor Drive Systems by Flying Capacitor Multilevel Inverter". In: *2018 International Power Electronics Conference (IPEC-Niigata 2018 -ECCE Asia)*. 2018, pp. 1972–1976. DOI: 10.23919/IPEC.2018.8507940.

[9] Reinaldo J. Perez. *Handbook of Aerospace Electromagnetic Compatibility*. Wiley-IEEE Press, 2018, pp. 249–286.

[10] Guochang Shi et al. "Methods of high intensity radiated field testing for civil aircraft". In: *2017 International Symposium on Electromagnetic Compatibility - EMC EUROPE*. 2017, pp. 1–6. DOI: 10.1109/EMCEurope.2017.8094704.

[11] C. R. Wilson and S. Grijalva. "An Analysis of the Susceptibility of Electric Aircraft to Lightning Strikes". In: *2021 IEEE Transportation Electrification Conference & Expo (ITEC)*. 2021, pp. 100–105. DOI: 10.1109/ITEC51675.2021.9490143.

[12] Richard Xian-Ke Gao et al. "Lightning Direct Effect and Electromagnetic Shielding Analysis of Conductive Aircraft Composite". In: *2019 International Symposium on Electromagnetic Compatibility - EMC EUROPE*. 2019, pp. 355–359. DOI: 10.1109/EMCEurope.2019.8872102.

[13] Maxim Solkin. "Electromagnetic interference hazards in flight and the 5G mobile phone: Review of critical issues in aviation security". In: *Transportation Research Procedia* 59 (2021), pp. 310 –318.

[14] Leonardo Malburg, Niek Moonen, and Frank Leferink. "The Changing Electromagnetic Environment Onboard All-Electric Aircraft, an EMC Perspective". In: *2021 IEEE International Joint EMC/SI/PI and EMC Europe Symposium*. 2021, pp. 845–850. DOI: 10.1109/EMC/SI/PI/EMCEurope52599.2021.9559208.

[15] *120° Square-Wave Commutation for Brushless DC Motors*. Toshiba Electronic Devices & Storage Corporation. Tokyo, Japan, 2018.

[16] *CY8CKIT-037 PSoC® 4 Motor Control Evaluation Kit Guide*. Cypress Semiconductor Corporation. San Jose, California, 2021.

[17] Shiyoung Lee, T.H. Lemley, and Gene Keohane. "A comparison study of the commutation methods for the three-phase permanent magnet brushless DC motor". In: 2009.

[18] Cadence PCB Solutions. *Common-Mode Voltage in Inverters: Effects and Reduction Methods*. URL: https://resources.pcb.cadence.com/blog/2022-common-mode-voltage-in-inverters-effects-and-reduction-methods. (Accessed: 2023-02-15).

[19] A. Kempski, R. Smolenski, and R. Strzelecki. "Common mode current paths and their modeling in PWM inverter-fed drives". In: *2002 IEEE 33rd Annual IEEE Power Electronics Specialists Conference. Proceedings (Cat. No.02CH37289)*. Vol. 3. 2002, 1551–1556 vol.3. DOI: 10.1109/PSEC.2002.1022396.

[20] Andrei Aursulesei. *Noise canceling methods in power inverters*. Bachelor's Thesis. University of Twente, 2019.

[21] Samarjeet Singh et al. "Analysis and Mitigation of the Common-Mode Noise in a Three-Phase SiC-Based Brushless DC Motor Drive With 120° Conduction Mode". In: *IEEE Transactions on Power Electronics* 37.5 (2022), pp. 5514–5523. DOI: 10.1109/TPEL.2021.3133880.

[22] Stephan Cordes and Frank Klotz. “Active common mode cancellation”. In: *2018 IEEE International Symposium on Electromagnetic Compatibility and 2018 IEEE Asia-Pacific Symposium on Electromagnetic Compatibility (EMC/APEMC)*. 2018, pp. 127–130. DOI: 10.1109/ISEMC.2018.8393752.

[23] Y.-C. Son and Seung-Ki Sul. “A new active common-mode EMI filter for PWM inverter”. In: *IEEE Transactions on Power Electronics* 18.6 (2003), pp. 1309–1314. DOI: 10.1109/TPEL.2003.818829.

[24] Shotaro Takahashi et al. “Common-Mode Voltage Attenuation of an Active Common-Mode Filter in a Motor Drive System Fed by a PWM Inverter”. In: *IEEE Transactions on Industry Applications* 55.3 (2019), pp. 2721–2730. DOI: 10.1109/TIA.2019.2892364.

[25] Shunsuke Ohara et al. “A novel active common-noise canceler combining feedforward and feedback control”. In: *2017 IEEE Energy Conversion Congress and Exposition (ECCE)*. 2017, pp. 2469–2475. DOI: 10.1109/ECCE.2017.8096473.

[26] Anaheim Automation. *BLY17*. URL: https://www.anaheimautomation.com/products/brushless/brushless-motor-item.php?sID=143&pt=i&tID=96&cID=22. (Accessed: 2023-02-25).

[27] James W. Nilsson and Susan Riedel. *Electric Circuits*. 9th ed. Pearson, 2010, pp. 274–275.

[28] E R Anagha, P V Nisha, and T K Sindhu. “Design of an active EMI filter for bearing current elimination in VFD”. In: *2018 IEEE International Symposium on Electromagnetic Compatibility and 2018 IEEE Asia-Pacific Symposium on Electromagnetic Compatibility (EMC/APEMC)*. 2018, pp. 131–134. DOI: 10.1109/ISEMC.2018.8393753.

[29] *IRFR3607PbF*. International Rectifier. Apr. 2010.

[30] *Ferrite - Summary*. TDK Electronics AG. 2021.

[31] *Ferrites and accessories: ETD 49/25/16, Core and accessories*. TDK Electronics AG. Oct. 2022.